

# Indentation analysis of sub-surface deformation in ductile materials after solid particle erosion

B.F. Levin, J.N. DuPont \*, A.R. Marder

*Department of Materials Science and Engineering, Lehigh University, Bethlehem, PA 18015, USA*

Received 13 September 1999; received in revised form 18 November 1999

## Abstract

Sub-surface deformation of several industrially important Ni, Co, and Fe-based wrought alloys and pure Cu, Ta, and Ni was analyzed. All samples were eroded by hard  $\text{Al}_2\text{O}_3$  particles at a  $90^\circ$  impact angle and  $40 \text{ m s}^{-1}$ . The deformation and load–displacement response within the plastically deformed zone below the eroded surface were measured by using a nanoindentation test system. Results from the indentation test were used to determine the effect of materials hardness on the restitution coefficient and to compare the amount of energy that is transferred into plastic deformation during particle impact. All materials showed a load–unload hysteresis, which represents a measure of the amount of energy dissipated into plastic deformation during indentation. Also, elastic recovery of the indenter was significantly higher near the eroded surface than away from the eroded surface. For all materials, a logarithmic-type relationship was observed between hardness and restitution coefficient. © 2000 Elsevier Science S.A. All rights reserved.

*Keywords:* Indentation analysis; Sub-surface deformation; Ductile materials; Solid particle erosion

## 1. Introduction

Erosion of ductile materials by the impact of hard solid particles at low and moderate velocities ( $2\text{--}100 \text{ m s}^{-1}$ ) can cause significant damage to structural components in many industrial applications. For example, erosion by non-combustible fly-ash particles causes premature material failures in the power generation industry. [1]. During impact on the elastic–plastic target, particle energy transfers into rebound and plastic deformation of the target [2]. Rebound of the particle is caused by the elastic energy stored in the particle and target material, and the magnitude of this energy is determined by the ratio of the rebound to the initial particle velocity. This ratio, called the restitution coefficient ( $e$ ), depends on the mechanical properties of the target material and erodent, and impact parameters (i.e. velocity, impact angle, and particle size). The extent of erosion damage is related to the ability of the material to elastically recover and therefore, it is important to

understand the effect of target mechanical properties, such as hardness, on the restitution coefficient.

Several studies have been conducted to measure the restitution coefficient of various target/erodent systems [2–4]. However, these measurements are complicated and often inaccurate because of the difficulties involved in measuring rebound velocity of the particle. Also, because of plastic deformation, mechanical properties of the target change with distance from the surface. Typically, the depth of the plastically deformed region ranges between 5 and  $200 \mu\text{m}$ , which makes it difficult to measure mechanical properties within this region using conventional methods. The objective of this study was to measure the restitution coefficients of several ductile materials within the plastically deformed region below the impacted surface by using the nanoindentation to perform small-scale indentation tests. Also, results from nanoindentation were used to determine the effect of hardness on the restitution coefficient of materials and to compare the amount of energy that is transferred into plastic deformation during particle impact.

\* Corresponding author. Tel.: +1-610-7583942; fax: +1-610-7584244.

Table 1  
Chemical compositions of the tested alloys (wt.%)

Alloy	Co	Cr	Fe	Mn	Mo	Ni	W	Ta	Cu	Other
Ultimet	Balance	25.5	3.0	0.8	4.3	8.9	1.3	–	–	0.24Si, 0.07C
Inconel 625	–	21.6	4.4	0.03	8.9	Balance	–	–	–	3.49Nb, 0.26Ti 0.15Al, 0.02C
Hastelloy C22	1.8	21.6	5.0	0.23	13.8	Balance	2.9	–	–	0.18V, 0.007C
Haynes 230	0.3	24.0	1.4	0.5	1.8	Balance	13.2	–	–	0.33Al, 0.07C, 0.43Si
316L SS	–	17.3	Balance	1.5	2.0	11.0	–	–	–	0.02C, 0.5Si
Haynes B3	–	1.2	–	0.54	27.2	Balance	–	–	–	0.34Al
Nickel 200	–	–	0.2	–	–	99.2	–	–	–	–
Tantalum	–	–	–	–	–	–	–	99.9	–	–
Copper	–	–	–	–	–	0.044	–	–	Balance	–

## 2. Experimental procedure

### 2.1. Materials

Several industrially important Ni, Co, and Fe-based wrought alloys (Ultimet, Inconel-625, Hastelloy-C22, Haynes-B3, Haynes-230, and 316L SS) and commercially pure Ta, Cu and Ni were chosen for this study. All of the alloys were solid-solution strengthened and provided a broad variation in mechanical properties. The chemical compositions were determined by optical emission spectroscopy and are shown in Table 1. Each material was obtained in the form of fully annealed, rolled bar stock, and the experiments discussed below were carried out on the materials in the as-received condition.

### 2.2. Erosion testing

The solid particle erosion testing apparatus used in this study is described in detail elsewhere [5]. All materials were tested at a 90° impact angle and a velocity of 40 m s<sup>-1</sup> and the standard test conditions chosen for this study are listed in Table 2. Each sample was mechanically polished to a 1-μm surface finish. Brown alumina (96% Al<sub>2</sub>O<sub>3</sub>, 3% TiO<sub>2</sub>), which has a size range from 355 and 425 μm, was used as an erodent. Fresh alumina particles (i.e. particles were not re-used) were used for the erosion tests. After the erosion tests, samples were cross-sectioned using a water cooled low speed diamond saw and mounted in cold curing, thermosetting epoxy. The samples were then metallographically prepared using standard techniques to produce a 0.04-μm surface finish and analyzed by nanoindentation to measure the sub-surface damage in the eroded materials.

### 2.3. Nanoindentation tests

Nanoindentation tests were performed using the Nano Indenter® II system, Fig. 1 [6]. The load on the indenter is generated through the use of a current

carrying coil and permanent magnet assembly. The resolution of the loading system is 50 nN. The displacement of the indenter is measured with a three plate capacitive system with a resolution of 0.04 nm. A detailed description of the system has been presented elsewhere [7]. In contrast to conventional microhardness tests, the system is able to measure the displacement of the indenter as a function of applied load within a small volume of material. The use of this depth-sensing indentation technique made it possible to analyze the load–displacement and stress–strain response of the material within the plastically deformed

Table 2  
Erosion tests conditions

Eroded sample planar dimensions	0.95 × 0.95 cm
Sample temperature	20°C
Erodent particle velocity	40 ± 3 m s <sup>-1</sup>
Erodent particles flux	8.50 mg mm <sup>-2</sup> s <sup>-1</sup>
Impingement angle	90°
Erodent	Angular brown alumina (Al <sub>2</sub> O <sub>3</sub> )
Erodent hardness	2000 HK <sub>10</sub>
Erodent size range	355–425 μm

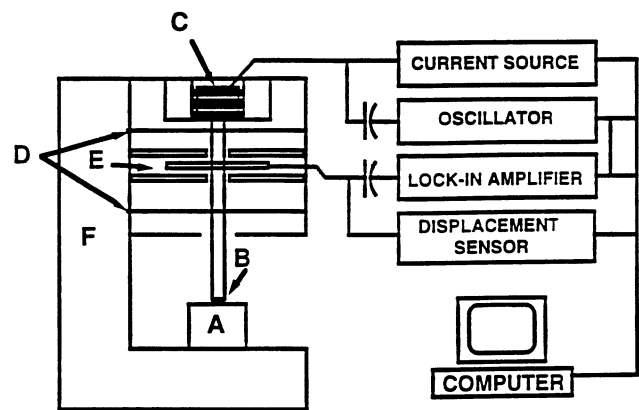


Fig. 1. Schematic diagram of the Nano Indenter® II. (A) Sample; (B) indenter column; (C) load applications coil; (D) indenter support springs; (E) capacitive displacement gauge; and (F) load frame.

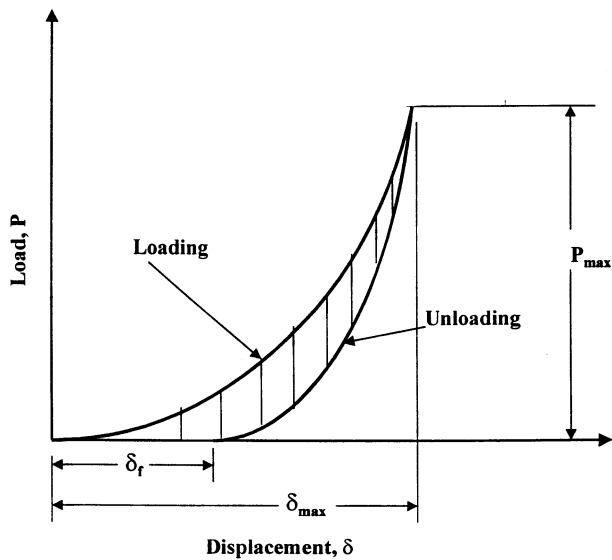


Fig. 2. Schematic diagram of the typical load–displacement curve obtained during the nanoindentation test. Shaded area represents plastic deformation energy,  $\delta_f$  is the final indentation depth after indentation, and  $\delta_{\max}$  is the maximum indentation depth at the peak load.

layer ( $< 150 \mu\text{m}$ ) below the deformed surface. These results provided an understanding of the energy absorption properties of the impacted materials.

The hardness was calculated according to the relationship  $H = P/A$ , where  $P$  is the maximum load and  $A$  is the projected area of the residual indentation. In this case,  $A = \pi a^2$ , where  $a$  is the radius of the residual indentation. In these experiments, the indenter penetration depth was small compared with the radius of the indenter. Therefore, the value of  $a$  can be found from the depth of the indenter penetration, which is directly measured using the Nanoindenter, according to  $a = (\delta R)^{0.5}$  [8], where  $\delta$  is the penetration depth and  $R$  is the indenter radius. Therefore, hardness can be found from the relation  $H = P/(\pi\delta R)$ .

### 2.3.1. Load–displacement measurements

A schematic diagram of the typical load–displacement curve that can be obtained by using the nanoindentation technique is shown in Fig. 2. As the load,  $P$ , increases, displacement occurs due to both elastic and plastic deformation of the material (loading curve). After the load is removed, the elastic displacement is recovered (unloading curve). Thus, because of the plastic deformation, a material exhibits contact hysteresis (i.e. some amount of energy that was transferred into the material during the loading cycle is absorbed through plastic deformation). The shaded area in Fig. 2 represents this plastic deformation energy.

Indentation tests were conducted with a  $50 \mu\text{m}$  radius diamond ball and a peak load of  $80 \text{ mN}$  on the cross-sections of all materials exposed to particle im-

pacts. For each indentation a load–displacement curve was generated. A loading/unloading rate of  $2 \text{ mN s}^{-1}$  and  $20 \text{ s}$  hold time at the peak load were used during the load–hold–unload cycle. Indents started at  $10 \mu\text{m}$  from the eroded surface and proceeded towards the unaffected material with  $25\text{-}\mu\text{m}$  steps. Therefore, a series of load–displacement diagrams was produced at various distances from the eroded surface for each material. Since the area under the load displacement curve represents the energy that the material absorbs during the indentation process, a profile of the ability of the eroded materials to absorb this energy within the plastically deformed region was obtained. Four profiles (five indents in each profile) were obtained in different locations of each material in order to improve the statistical significance of the data.

Because of particle impacts, the material at and below the eroded surface deforms plastically and work hardens, and the material closest to the surface experiences the largest increase in hardness due to plastic deformation. This produces a gradient in mechanical properties with distance from the surface. In this work, a plastic zone depth is defined as the length of material below the eroded surface that has undergone an increase in hardness due to plastic deformation induced by the particle impacts. Plastic zone depths were estimated by obtaining a hardness profile from the eroded surface into the base material on the cross-sectioned samples. The depth below the eroded surface at which the hardness value becomes constant is defined as the plastic zone size. More details on this procedure can be found in reference [9].

## 3. Results and discussion

### 3.1. Theoretical basis for the indentation load–displacement analysis

#### 3.1.1. Elastic recovery analysis

During loading, the work done by the indenter in deforming the material is given by:

$$W = \int_0^{\delta} P(\delta) d\delta \quad (1)$$

where  $W$  is work done by the indenter,  $P$  is the applied load,  $\delta$  is the depth of penetration, and  $\delta_{\max}$  is the maximum depth of penetration at the highest load. The work  $W$  is represented as the area under the loading curve in Fig. 2. During unloading, the recovered elastic energy ( $W_{\text{elastic}}$ ) is given by:

$$W_{\text{elastic}} = \int_{\delta_{\text{final}}}^{\delta_{\max}} P(\delta) d\delta \quad (2)$$

where  $\delta_{\text{final}}$  is the depth of the residual indentation. In Fig. 2, the elastically recovered energy is represented as

the area under the unloading curve. If the indenter is regarded as a free particle, the coefficient of restitution ( $e = V_{\text{rebound}}/V$ ) can be found according to [10]:

$$e = \left( \frac{W_{\text{elastic}}}{W} \right)^{0.5} \quad (3)$$

$$e^2 = \frac{W_{\text{elastic}}}{W} \quad (4)$$

Assuming that the impacting particle does not fracture or deform upon impact, the portion of its kinetic energy that is transferred into plastic deformation of the target is given by:

$$\text{KE}_{\text{plastic}} = mV_{\text{initial}}^2 \left( 1 - \frac{V_{\text{rebound}}^2}{V_{\text{initial}}^2} \right) = mV_{\text{initial}}^2 (1 - e^2) \quad (5)$$

where  $V_{\text{initial}}$  is the initial velocity of the particle,

$V_{\text{rebound}}$  is the rebound velocity of the particle, and  $m$  is the mass of the particle. Therefore, if the restitution coefficient ( $e$ ) can be measured from the load–displacement tests (Eqs. (3) and (4)), the amount of energy transferred into plastic deformation of the target can be determined. Also, results from the nanoindentation tests can be used to (1) determine the effect of hardness on the restitution coefficient of materials and (2) compare the amount of energy that is transferred into plastic deformation during particle impact of different materials.

### 3.2. Measurements of subsurface elastic recovery and plastic deformation

Results of the load–displacement tests conducted on cross-sections of the eroded materials are presented in

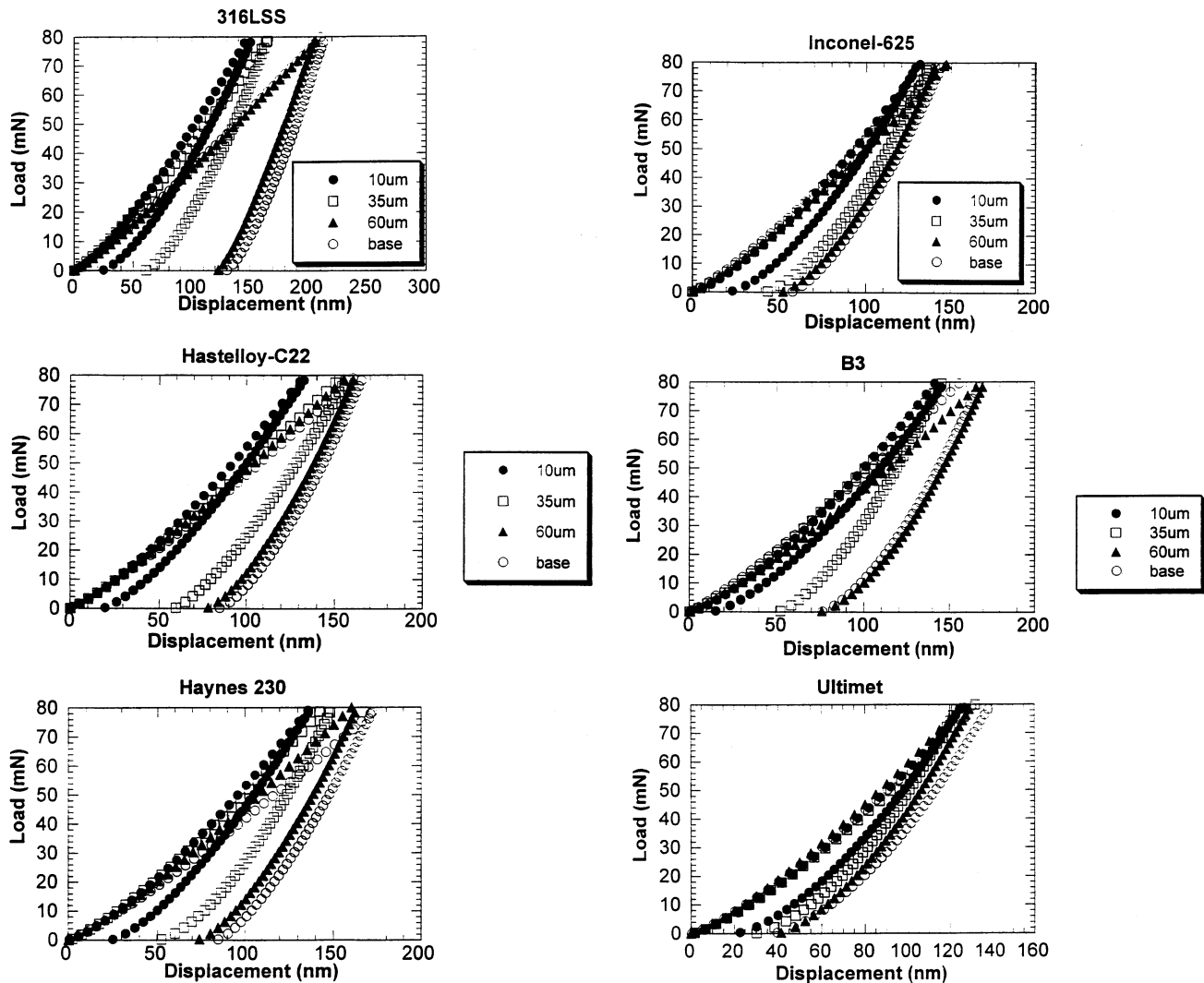


Fig. 3. Indentation load,  $P$ , versus displacement,  $\delta$ , for tested materials as a function of distance from the eroded surface. Measurements were made on the cross-sections of the eroded materials ( $90^\circ$  particle impact angle and velocity of  $40 \text{ m s}^{-1}$ ). Note an increase in elastic recovery near the eroded surface.

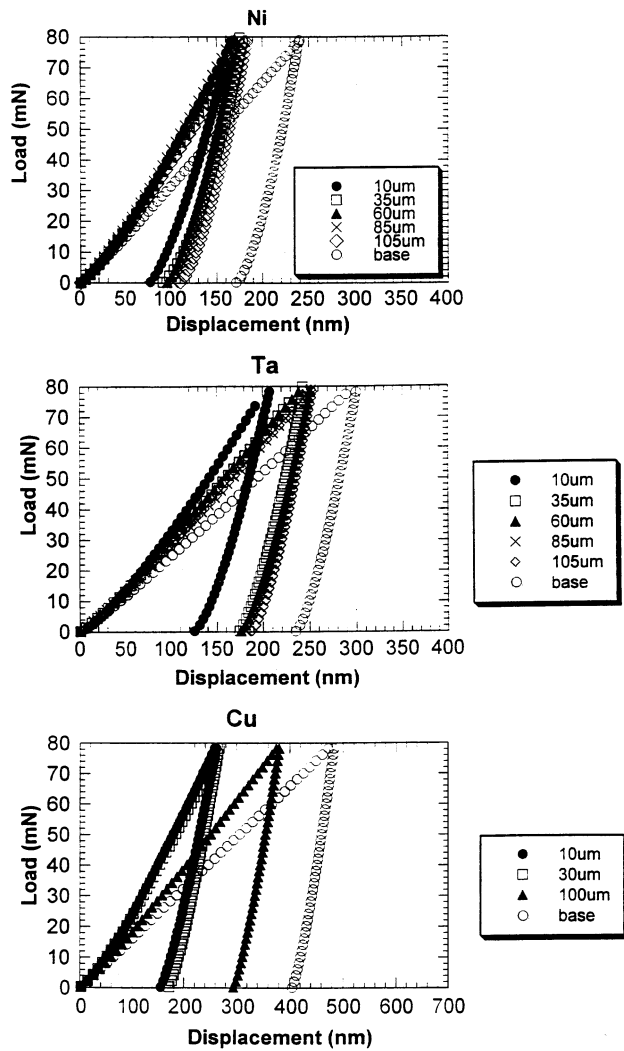


Fig. 3. (Continued)

Fig. 3. Two observations can be made from the data. First, all materials showed a load–unload hysteresis that represents a measure of the amount of energy dissipated into plastic deformation during indentation. Second, elastic recovery ( $W_{\text{elastic}}/W$ ) was significantly higher near the eroded surface than away from the eroded surface. Subsequently, energy that is dissipated into plastic deformation,  $W_{\text{plastic}}$ , decreased near the eroded surface and the materials became less ductile. Table 3 lists the values of  $W_{\text{plastic}}$  and  $W_{\text{elastic}}/W$  or  $e^2$  for all tested materials. Average values of  $e^2$  within the plastic zone were determined using the following equation:

$$\text{average } e^2 = \frac{\int_0^{L_{\text{pl}}} e^2(L) dL}{L_{\text{pl}}} \quad (6)$$

where  $L_{\text{pl}}$  is the plastic zone size due to erosion. Table 3 shows that, near the eroded surface (10  $\mu\text{m}$ ), anywhere from 36 to 88% of total energy is elastically recovered during unloading cycle. Tantalum showed the lowest elastic recovery ( $e^2 = 0.36$ ) while the B3 alloy showed the highest elastic recovery ( $e^2 = 0.88$ ). On average, between 27 and 72% of total energy is recovered during the unloading cycle. These findings are important because often researchers assumed that during particle impact, only 5–10% of the total energy transfers into elastic recovery (particle rebound) and 90–95% transfers into plastic deformation of the target [11]. Therefore, elastic recovery has been largely ignored in energy balance calculations. This research suggests that elastic recovery can play a substantial role in the total energy loss and thus, must be considered in the energy balance calculations. Also, within the plastically deformed region, all materials exhibited an increase in restitution coefficient with an increase in hardness near the eroded surface. At this point, it is appropriate to discuss the correlation between the values of the restitution coefficient measured by quasi-static indentation tests and those expected during impact testing.

Latham et al. [12] measured rebound velocity and coefficient of restitution ( $V_{\text{rebound}}/V$ ) of several annealed metals impacted by iron microspheres (0.1–2  $\mu\text{m}$  in diameter). They found that, in the impact velocity range 20–100  $\text{m s}^{-1}$ , average  $e^2$  values for annealed Cu, Ni, and stainless steel were 0.12, 0.10, and 0.3, respectively. Also, the restitution coefficient values did not significantly vary with impact velocity. These values are in reasonable agreement with those measured using a quasi-static nanoindentation technique for base Cu, Ni, and 316L stainless steel (0.15, 0.2, and 0.36, respectively). This suggests that, in the low impact velocity range, the incident velocity of the particle does not significantly influence the restitution coefficient. Also, Johnson [13] derived that, when fully plastic conditions are obtained during impact,  $e$  is proportional to  $V^{-1/4}$ , which would explain the relative insensitivity of the restitution coefficient with incident velocity. Therefore, the load–displacement indentation technique provides the ability to estimate the restitution coefficient and can be used to estimate energy loss during particle impact. In addition, if the particle does not deform upon impact and is harder than the target material, the analogy between the indenter and a particle can be reasonable. Furthermore, the indenter and particle can cause plastic deformation of the target during contact. However, the effect of the particle size on restitution coefficient of the target/particle system has not been thoroughly investigated and thus, could contribute to differences between the measured restitution coefficient during impact and indentation tests.

### 3.2.1. Effect of hardness on restitution coefficient and plastic deformation energy

The effect of hardness on measured restitution coefficient is shown in Fig. 4. Interestingly, the data for all materials and distances from the eroded surface (see Table 3) can be fitted into a logarithmic-type relationship ( $R^2 = 0.94$ ):

$$e = -0.68 + 0.39 \log(H) \quad (7)$$

where  $H$  is hardness in MPa. This result is somewhat

different from that obtained by Latham et al. [12] who showed a linear relationship between Vickers hardness and restitution coefficient (Fig. 5). However, upon examining Fig. 5, it can be seen that the hardest tested material was graphite with Vickers hardness of only 400 kg mm<sup>-2</sup> (4000 MPa). In this study (Fig. 4), for materials with hardness below 4000–5000 MPa, the relationship between  $H$  and  $e$  could also be described as linear. However, materials with hardness greater than 5000 MPa deviated from the linear relationship. At the same applied load, hard materials have a smaller de-

Table 3

Summary of the load–displacement data for eroded materials. Particle impact angle-90° and velocity-40 m s<sup>-1</sup>

Material	Distance from the eroded surface, μm	Plastic zone depth, μm	Plastic energy, $W_{\text{plastic}}, \text{J} \times 10^{-9}$	Total energy, $W \text{ J} \times 10^{-9}$	Measure of elastic recovery, $W_{\text{elastic}}/W$ or $e^2$	Average $e^2$ within the deformed volume
Cu	10	140	5.54	9.43	0.41	0.28
	35		6.17	9.64	0.36	
	105		11.50	14.59	0.21	
	Base <sup>a</sup>		16.41	19.28	0.15	
Ta	10	110	4.83	7.57	0.36	0.27
	35		6.86	9.32	0.26	
	60		7.36	10.12	0.27	
	85		7.45	9.82	0.24	
	105		7.55	9.75	0.23	
	Base		9.38	11.50	0.18	
Ni	10	80	2.87	6.11	0.53	0.40
	35		3.68	6.43	0.43	
	60		3.61	6.22	0.42	
	85		3.96	6.40	0.38	
	Base		7.14	9.64	0.26	
316L SS	10	60	1.09	5.52	0.80	0.58
	35		2.74	6.60	0.58	
	60		4.85	8.20	0.41	
	Base		5.23	8.30	0.36	
Hastelloy-C22	10	50	0.83	5.13	0.84	0.66
	35		2.40	5.84	0.59	
	60		3.24	6.06	0.47	
	Base		3.48	6.29	0.45	
Haynes 230	10	50	0.96	4.96	0.80	0.65
	35		2.28	5.55	0.60	
	60		2.98	6.00	0.50	
	Base		3.30	6.51	0.49	
B3	10	40	0.61	5.03	0.88	0.7
	35		2.02	5.34	0.62	
	60		3.09	6.09	0.49	
	Base		3.24	6.31	0.47	
Inconel 625	10	50	0.84	4.65	0.82	0.71
	35		1.91	5.17	0.63	
	60		2.15	5.30	0.59	
	Base		2.28	5.44	0.58	
Ultimet	10	40	0.90	4.51	0.80	0.72
	35		1.55	4.57	0.66	
	60		1.66	4.72	0.65	
	Base		1.81	5.25	0.65	

<sup>a</sup> Base measurements were made on unaffected material away from the eroded surface ( $\approx 500 \mu\text{m}$ ).

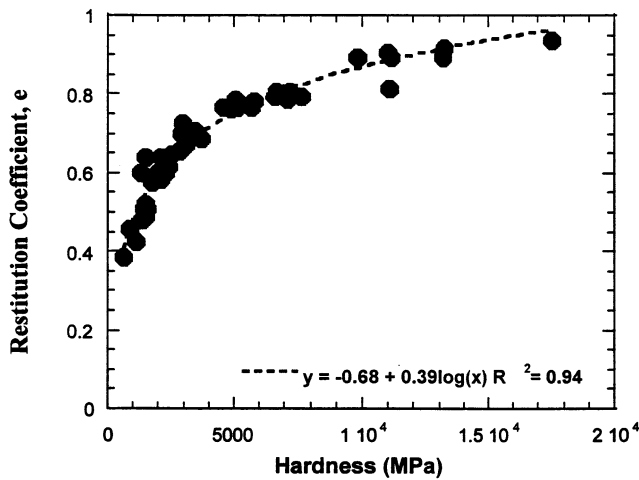


Fig. 4. The effect of hardness on restitution coefficient,  $e$ , measured from the load–displacement experiments. The data for all materials and distances from the eroded surface can be fitted into a logarithmic-type relationship.

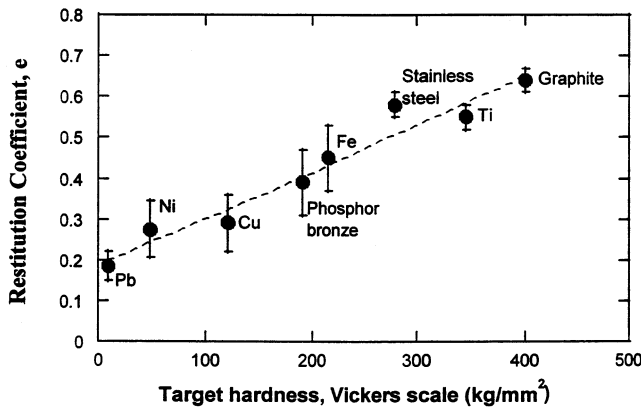


Fig. 5. Dependence of the restitution coefficient,  $e$ , within the velocity range 20–100 m s<sup>-1</sup> on the Vickers hardness of target materials. The error bars associated with each point represent the variation of  $e$  over this velocity range.

formed volume beneath the indenter than soft materials. It can be suggested that, at some level of hardness, the size of the deformed region becomes comparable with the size of the dislocation stress field generated by the indentation. Tabor [14] suggested that, when the deformed volume is very small, it may contain only a limited number of dislocations and one should expect the hardness of material to approach the theoretical value of a perfect crystal. Therefore, changes and any further increase in material hardness will not produce a significant increase in elastic recovery. However, near the eroded surface all materials were highly hardened and, therefore, it is unlikely that during indentation experiments only a limited number of dislocations were affected. It seems that, when

indentation size becomes small, the dislocation stress field may affect energy dissipation during indentation.

#### 4. Conclusions

Subsurface deformation behavior of ductile Ni, Co, and Fe-base alloys and commercially pure Ni, Cu, and Ta exposed to solid particle erosion (90° particle impact angle and velocity of 40 m s<sup>-1</sup>) was analyzed. Nanoindentation was used to determine load–displacement and stress–strain response of materials below the eroded surface. The results are summarized as follows:

A nanoindentation method was utilized to estimate the restitution coefficient within plastically deformed regions of eroded samples that provides a measure of the rebounding ability of a material during particle impact.

An increase in hardness ( $H$ ) of tested to an increase in restitution coefficient ( $e$ ) according to the logarithmic-type relationship:  $e = -0.68 + 0.39 \log(H)$ . Consequently, the increase in hardness produced a decrease in amount of plastic deformation dissipated into the material.

#### Acknowledgements

Research sponsored by the Assistant Secretary for Energy Efficiency and Renewable Energy, Office of Transportation Technologies, as part of the High Temperature Materials Laboratory User Program, Oak Ridge National Laboratory, managed by Lockheed Martin Energy Research Corp. for the US Department of Energy under contract number DE-AC05-96OR22464. The authors would also like to thank K. Breder and L. Riester from High Temperature Materials Laboratory, Oak Ridge National Laboratory, Oak Ridge, TN for their help in conducting indentation experiments and valuable discussions.

#### References

- [1] L. Lammarre, EPRI J. October/November (1990) 31.
- [2] Y. Tirupataiah, B. Venkataraman, G. Sundarajan, Mater. Sci. Eng. A124 (1990) 133–140.
- [3] W. Tabakoff, J. Propulsion 7 (5) (1991) 805–813.
- [4] M. Metwally, W. Tabakoff, A. Hamed, J. Eng. Gas Turbines Power 117 (1995) 213–219.
- [5] B. Lindsley, K. Stein, A.R. Marder, Measurement Sci. Technol. 6 (1995) 1169–1174.
- [6] W.C. Oliver, G.M. Pharr, J. Mater. Res. 7 (6) (1992) 1564–1583.
- [7] M.F. Doerner, W.D. Nix, J. Mater. Res. 1 (1986) 601.

- [8] J.S. Field, M.V. Swain, *J. Mater. Res.* 8 (2) (1993) 297–306.
- [9] B.F. Levin, J.N. DuPont, A.R. Marder, *Wear* 181–183 (1995) 810–820.
- [10] R.F. Cook, G.M. Pharr, *J. Hard Mater.* 5 (1994) 179–190.
- [11] I.M. Hutchings, *Wear* 70 (1981) 269–281.
- [12] R.V. Latham, A.S. Brah, K. Fok, Woods, *J. Phys. D. Appl. Phys.* 10 (1977) 139–150.
- [13] K.L. Johnson, *Contact Mechanics*, Cambridge University Press, Cambridge, 1985, p. 363.
- [14] D. Tabor, *The Hardness of Metals*, Clarendon Press, Oxford, 1951.